Monthly Notices of the Royal Astronomical Society
MNRAS **507**, 919–926 (2021) https://doi.org/10.1093/mnras/stab2154
Advance Access publication 2021 July 31

Hubble diagram at higher redshifts: model independent calibration of quasars

Xiaolei Li,[1⋆] Ryan E. Keeley,[2⋆] Arman Shafieloo,[2,3⋆] Xiaogang Zheng,[4] Shuo Cao,[5] Marek Biesiada[5,6] and Zong-Hong Zhu[5]

[1] *College of Physics, Hebei Normal University, Shijiazhuang 050024, China*
[2] *Korea Astronomy and Space Science Institute, Daejeon 34055, Korea*
[3] *University of Science and Technology, Yuseong-gu 217 Gajeong-ro, Daejeon 34113, Korea*
[4] *School of Electrical and Electronic Engineering, Wuhan Polytechnic University, Wuhan 430023, China*
[5] *Department of Astronomy, Beijing Normal University, Beijing 100875, China*
[6] *National Centre for Nuclear Research, Pasteura 7, PL-02-093 Warsaw, Poland*

Accepted 2021 July 21. Received 2021 July 21; in original form 2021 April 23

ABSTRACT

In this paper, we present a model-independent approach to calibrate the largest quasar sample. Calibrating quasar samples is essentially constraining the parameters of the linear relation between the log of the ultraviolet (UV) and X-ray luminosities. This calibration allows quasars to be used as standardized candles. There is a strong correlation between the parameters characterizing the quasar luminosity relation and the cosmological distances inferred from using quasars as standardized candles. We break this degeneracy by using Gaussian process regression to model-independently reconstruct the expansion history of the Universe from the latest type Ia supernova observations. Using the calibrated quasar data set, we further reconstruct the expansion history up to redshift of $z \sim 7.5$. Finally, we test the consistency between the calibrated quasar sample and the standard Lambda cold dark matter (ΛCDM) model based on the posterior probability distribution of the GP hyperparameters. Our results show that the quasar sample is in good agreement with the standard ΛCDM model in the redshift range of the supernova, despite the $2-3\sigma$ significant deviations taking place at higher redshifts. Fitting the standard ΛCDM model to the calibrated quasar sample, we obtain a high value of the matter density parameter $\Omega_m = 0.382^{+0.045}_{-0.042}$, which is marginally consistent with the constraints from other cosmological observations.

Key words: Cosmology: observations – quasars: general – Methods: statistical.

1 INTRODUCTION

As a potential cosmic probe at higher redshifts, quasars might be able to fill the redshift gap between the farthest observed Type Ia supernovae (SN Ia; Scolnic et al. 2017) and the cosmic microwave background (CMB; Aghanim et al. 2020) owing to the fact that quasars are luminous persistent sources in the Universe and can be observed up to redshifts of $z \approx 7.5$ (Mortlock et al. 2011). For instance, recently it has been proposed that intermediate-luminosity radio quasars could potentially provide a new type of standard rulers, which extended our understanding of the evolution of the Universe to $z \sim 3$ (Cao et al. 2017b, a, 2018; Li et al. 2017; Qi et al. 2019, 2021). More interestingly, quasars have also been used as standard candles whose standardization relies on the linear relation between the log of their ultraviolet (UV) and X-ray luminosities (Risaliti & Lusso 2015, 2017; Lusso & Risaliti 2016, 2017; Risaliti & Lusso 2019; Salvestrini et al. 2019; Lusso et al. 2019, 2020; Lusso 2020; Khadka & Ratra 2020a, b; Liu et al. 2020a, b, c; Geng et al. 2020; Zheng et al. 2021).

So far, the largest quasar sample with both X-ray and UV observations consists of ∼12 000 objects, assembled by combining several different samples in Lusso et al. (2020). The full sample includes 29 quasars from *XMM–Newton* at $z \simeq 3$ (Nardini et al. 2019); 1 new optically selected quasar at $z \sim 4$ from *XMM–Newton* (Nardini et al. 2019); 64 high-z quasars from Salvestrini et al. (2019); 840 quasars from the XMM-XLL sample published by Menzel et al. (2016); 9252 quasars from the SDSS-4XMM sample (Mingo et al. 2016; Pâris et al. 2017; Webb et al. 2020); 2392 quasars from Pâris et al. (2017), Evans et al. (2010); and 15 local AGN selected from Lusso et al. (2020). Note that several filtering steps were applied to reduce the systematic effects and 2421 quasars in the redshift range $0.009 < z < 7.5$ were left in the final cleaned sample (Lusso et al. 2020). The relation between the X-ray and UV luminosities is usually parametrized as $\log(L_X) = \gamma \log(L_{UV}) + \beta_1$, where L_X and L_{UV} are the rest-frame monochromatic luminosities at 2 keV and 2500 Å, respectively (Avni & Tananbaum 1986). There is a total of three free parameters for the quasar calibration, the slope of the relation γ, the offset of the relation β_1, and the intrinsic dispersion δ, which is not shown directly in the equation.

Up to now, different methods have been used to calibrate quasar samples. In Risaliti & Lusso (2015), the authors obtained the best-fitting values of γ and β_1 based on the ΛCDM model. The parameter

⋆ E-mail: lixiaolei@hebtu.edu.cn (XL); rkeeley@kasi.re.kr (REK); shafieloo@kasi.re.kr

β_1 shifts the relation between the UV and X-ray luminosities up and down and thus also scales the corresponding distance-redshift relation up and down. When doing cosmological inference, β_1 is thus degenerate with Hubble constant H_0 and only a combination of the two can be measured but not either individually. One way to calculate the value of γ was carried out in Risaliti & Lusso (2019), in which the authors split the quasar sample into subsamples within narrow redshift bins and then fit the linear $\log(F_{\rm UV})-\log(F_{\rm X})$ relation in each redshift bin. In this way, an average value of γ was obtained in the end. In this work, we introduce a novel model-independent technique to calibrate the quasar sample, in which we use Gaussian process (GP) regression to reconstruct the expansion history from the Pantheon SN Ia data set Scolnic et al. (2017). We then use these reconstructions of the unanchored luminosity distances ($D_{\rm L}H_0$) to break the degeneracy between the parameters of the quasar calibration and the expansion history, thus calibrating the quasars in a way that are, by construction, consistent with the SN Ia and independent of any cosmological or parametric assumption. It should be emphasised here that, all the work is done based on the assumption that there is no evolution of the $L_{\rm UV}-L_{\rm X}$ relation with redshift and this assumption has been tested in the previous works.

This paper is organized as follows. In Section 2, we describe the model-independent quasar calibration method in detail and show the Hubble diagram of the calibrated quasars. We test the reliability of the calibration results in Section 3. In Section 4, we constrain the ΛCDM model with the calibrated quasar sample. We reconstruct the expansion history with GP from the calibrated quasar sample with the best-fitting ΛCDM model as a mean function and test the consistency between the calibrated quasar sample and the ΛCDM model in Section 5. We discuss our conclusions in Section 6.

2 CALIBRATION

Here, we calibrate the 2421 quasar sample, which was compiled in Lusso et al. (2020). In this section, we describe the calibration method in detail and show the calibration results. Moreover, the reliability of the calibration results are also discussed in the next section.

From the linear relation between $\log(L_{\rm UV})$ and $\log(L_{\rm X})$, $\log(L_{\rm X}) = \gamma\log(L_{\rm UV}) + \beta_1$, one can obtain

$$\log(F_{\rm X}) = \gamma\log(F_{\rm UV}) + (2\gamma-2)\log(D_{\rm L}) + \beta_2, \tag{1}$$

where $\beta_2 = \gamma\log(4\pi) - \log(4\pi) + \beta_1$, $F_{\rm UV}$ and $F_{\rm X}$ are the fluxes measured at fixed rest-frame wavelengths, and $D_{\rm L}$ is the luminosity distance. In order to calibrate the quasar parameters in a model-independent way, an external observation is needed. In other words, since the quasar calibration parameters are degenerate with the cosmological distances, if we use the cosmological distances from another tracer of the expansion history (i.e. SN Ia), we can break this degeneracy and tightly constrain the calibration parameters. During our work, we generate samples of the unanchored luminosity distance $D_{\rm L}H_0$ from the posterior of the Pantheon compilation from Scolnic et al. (2017) calculated with GP [see Liao et al. (2019, 2020) for details on this sampling and see Rasmussen & Williams (2006), Holsclaw et al. (2010a, b, 2011), Shafieloo, Kim & Linder (2012), Joudaki et al. (2018), Keeley et al. (2019, 2020, 2021) for a broader discussion of GP].

As a reminder, since the absolute brightness of the SN Ia is degenerate with H_0, only the dimensionless, unanchored luminosity distances ($D_{\rm L}H_0$) can be measured.

GP regression works by generating a set of cosmological functions from the covariance function between the values at different redshifts. We follow some previous works and assume that the covariance function is parametrized as a squared-exponential kernel (Rasmussen & Williams 2006; Holsclaw et al. 2010a, b; Holsclaw et al. 2011; Shafieloo et al. 2012):

$$\left\langle\varphi(s_i)\varphi(s_j)\right\rangle = \sigma_f^2\exp\left(-\frac{|s_i-s_j|^2}{2\ell^2}\right) \tag{2}$$

where $s_i = \ln(1+z_i)/\ln(1+z_{\rm max})$ and $z_{\rm max} = 2.26$ is the maximum redshift of the SN Ia sample. There are two hyperparameters, σ_f and ℓ, that are marginalized over. These hyperparameters determine the amplitude of the random fluctuations and the coherence length of the fluctuation, respectively. φ is just a random function drawn from the distribution defined by the covariance function of equation (2) and we take this function as $\varphi(z) = \ln(H^{\rm mf}(z)/H(z))$, i.e. the logarithm of the ratio between the reconstructed expansion history, $H(z)$, and a mean function, $H^{\rm mf}(z)$, which we choose to be the best-fitting ΛCDM model from Pantheon data set. The mean function plays an important role in GP regression and the final reconstruction results are not quite independent of the mean function; however, it has a modest effect on the final reconstruction results because the values of hyperparameters help to trace the deviations from the mean function (Shafieloo et al. 2012; Shafieloo, Kim & Linder 2013; Aghamousa, Hamann & Shafieloo 2017). Moreover, the true model should be very close to the flat ΛCDM model so it is reasonable to choose the best-fitting flat ΛCDM model from Pantheon as a mean function.

With the reconstructed expansion history $H(z)$, we can integrate this function to get the unanchored luminosity distance,

$$D_L H_0(z) = (1+z)\int_0^z {\rm d}z\frac{c}{h(z)}, \tag{3}$$

where $h(z) = H(z)/H_0$. It is this function that is most directly constrained by the SN Ia data and can thus be reconstructed. GP effectively calculates a posterior for this function,

$$P(D_L H_0(z)|D) = \int d\varphi\mathcal{L}(D_L H_0(\varphi))P(\varphi)/P(D), \tag{4}$$

using the likelihood of the data $\mathcal{L}(D_L H_0(\varphi))$ (see equation 6) and a prior on φ (which is a consequence using a flat prior on the GP hyperparameters σ_f and ℓ). It is from this posterior distribution that we draw samples of the unanchored luminosity distance.

With the GP results in hand, the first step in calibrating the quasar distances is to draw 1000 unanchored luminosity distances $D_{\rm L}H_0$ reconstructed from the SN Ia data. We then calculate the predicted quasar X-ray flux corresponding to these unanchored luminosity distances $D_{\rm L}H_0$ by rewriting equation (1) as,

$$\log(F_{\rm X})^{\rm SN} = \gamma\log(F_{\rm UV}) + (2\gamma-2)\log(D_{\rm L}H_0) + \beta, \tag{5}$$

where $\beta = \beta_2 - (2\gamma-2)\log(H_0)$. With the measurements of $F_{\rm UV}$ and the $D_{\rm L}H_0$ from SN Ia, we obtain $\log(F_{\rm X})^{\rm SN}$ following equation (5). This allows us to compare the quasar data set and the SN Ia data set.

Then, following Risaliti & Lusso (2015) and Lusso et al. (2020), we define the likelihood ($\mathcal{L} = \exp\left(-\chi^2/2\right)$) of the quasar parameters based on a modified χ^2 function, which includes a penalty term for the intrinsic dispersion δ

$$\chi^2 = \sum_i\left[\frac{\left(\log(F_{\rm X}(\gamma,\beta))_i^{\rm SN} - \log(F_{\rm X})_i^{\rm QSO}\right)^2}{s_i^2} + \ln\left(s_i^2\right)\right], \tag{6}$$

where $s_i^2 = \sigma^2_{\log(F_{\rm X})} + \gamma^2\sigma^2_{\log(F_{\rm UV})} + \delta^2$. The intrinsic dispersion δ of the $L_{\rm L}-L_{\rm UV}$ relation is considered in order to reduce the Eddington bias that has the effect of flattening the $L_{\rm L}-L_{\rm UV}$ relation (Risaliti & Lusso 2019; Lusso et al. 2020). Further, a non-zero value for this parameter is needed in order yield a reasonable χ^2 per degree of

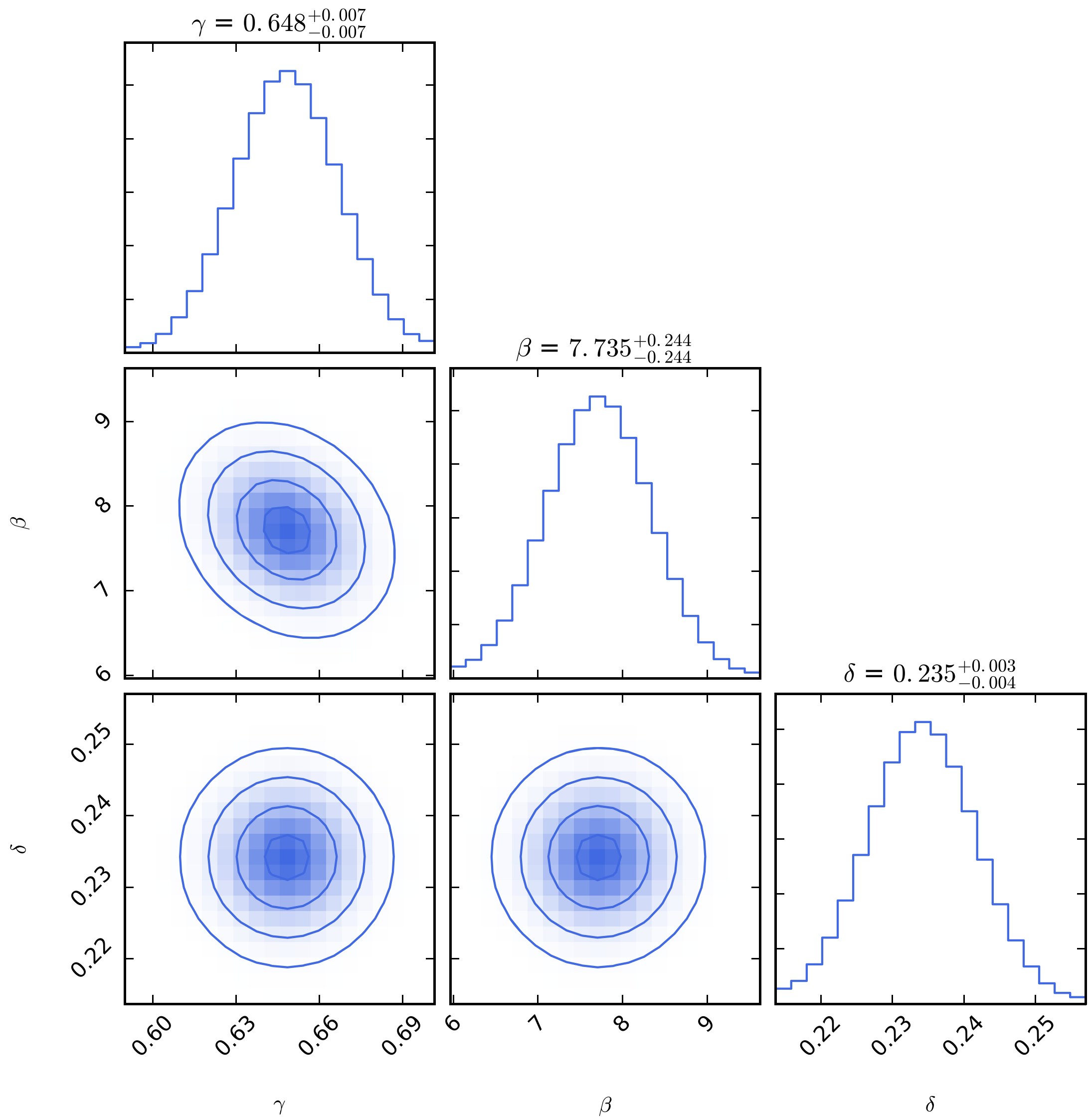

Figure 1. Model-independent calibration results for the quasar parameters. GP reconstructions of $D_L H_0$ based on the Pantheon SN Ia compilation were used. The contours represent the 1σ, 2σ, and 3σ uncertainties for γ, β, and δ. Marginal distributions for each parameter are shown on the top of each 2D subplot.

freedom. The observed dispersion of the X-ray fluxes is far larger than just the measurement error, so there must be some additional variance that is an intrinsic feature of the quasar population, and not the measurement of them. We account for this intrinsic scatter with the parameter δ. With equation (6), we use the **LINMIX_ERR** method (Kelly 2007), which accounts for measurements uncertainties on both independent and dependent variables, non-detections, and intrinsic scatter. The penalty term is important to guard against the intrinsic dispersion growing too large in the fit. For example, simply minimizing the χ^2 can be trivially achieved with a sufficiently large value of δ. However, the χ^2 per degree of freedom in this case would be close to zero, not one. Thus, the penalty term assures that δ is only as large as it needs to be to make the residuals Gaussian distributed (χ^2 per degree of freedom $\sim$1). We then calculate the posterior distribution of the quasar parameters: the slope γ, the intercept β and the intrinsic dispersion parameter δ. We should note that the Hubble constant H_0 is absorbed into the parameter β. Based on the method described above, we use a Python package named *emcee* (Foreman-Mackey et al. 2013) to do the MCMC analysis and flat priors are used for each parameter.

Our calibration method can be summarized as follows:

(i) Draw 1000 unanchored luminosity distances $D_{\rm L}H_0$ from supernovae data,
(ii) Calculate the predicted quasar X-ray flux corresponding to these unanchored luminosity distances,
(iii) Define the likelihood of the quasar parameters,
(iv) Calculate the posterior distribution of the quasar parameters.

The best-fitting values for quasar parameters γ, β, and δ and 1σ, 2σ, and 3σ uncertainties are shown in Fig. 1. We find that $\gamma = 0.649 \pm 0.007$ and $\delta = 0.235 \pm 0.04$. One can see that our constraints on the slope parameter γ and the intrinsic dispersion parameter are consistent at the 1σ confidence level with the calibration results from Lusso et al. (2020) that gives $\gamma = 0.586 \pm 0.061$, $\delta = 0.21 \pm 0.06$ by dividing the sample in redshift bins and fitting the $F_{\rm X}$–$F_{\rm UV}$ relation in the chosen redshift bins. The intercept parameter β is a function of both β_1 and H_0 and represents the relative anchoring between the unanchored luminosity distances and the observed

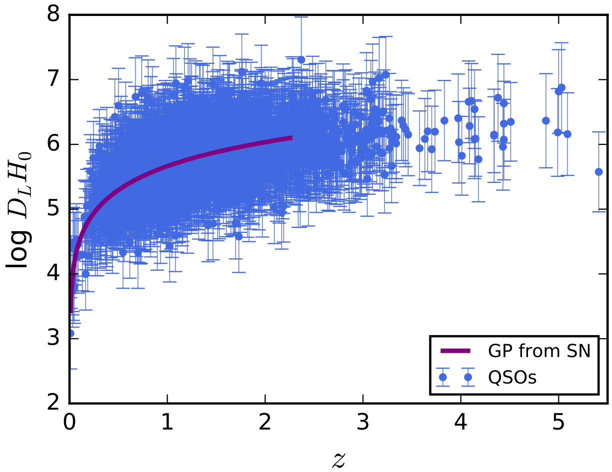

Figure 2. $\log(D_{\rm L}H_0)$–redshift relation for the 2421 calibrated quasars. The errorbars of $\log(D_{\rm L}H_0)$ are obtained through error propagation and the purple solid line shows $\log(D_{\rm L}H_0)$ drawn from the posterior of the Pantheon compilation calculated with GP.

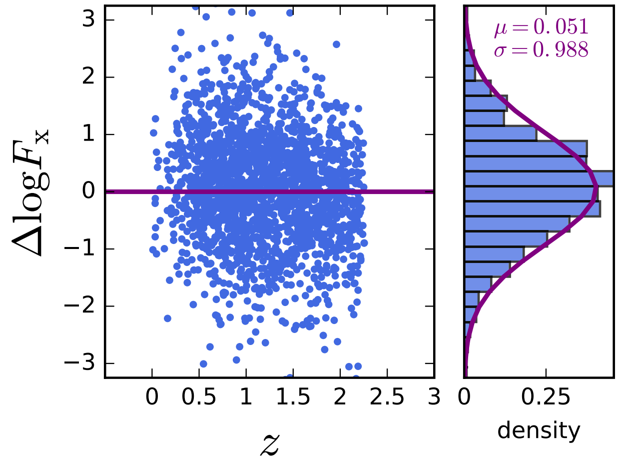

Figure 3. Residuals of the observed $\log(F_{\rm X})$ values with respect to the predicted $\log(F_{\rm X})$ values derived from the GP reconstructions of the Pantheon SN Ia compilation, normalized to the calibrated errors (observational and intrinsic). The right plot shows the histogram for $\Delta\log(F_{\rm X})$ and the purple line shows the best Gaussian fit with $\mu = -0.051$ and $\sigma = 0.988$.

quasar fluxes. It has absorbed all of the information about the anchoring of the data and other anchoring of the model.

3 TESTING THE INTERNAL CONSISTENCIES

With the best fits for the quasar parameters γ, β, and δ, we can then calculate a series of checks to be sure the calibration results infer reasonable information about cosmology. For instance, the $\log(D_{\rm L}H_0)$ versus z relation can be obtained from the quasar fluxes and calibrated quasar parameters via

$$\log(D_{\rm L}H_0) = \frac{\log(F_{\rm X}) - \gamma\log(F_{\rm UV}) - \beta}{(2\gamma - 2)}. \tag{7}$$

Fig. 2 shows the $\log(D_{\rm L}H_0)$ versus z relation for the 2421 quasar sample, together with the median inference from the posterior of the Pantheon compilation calculated with GP regression, which is shown by the purple solid line. The blue points represent the quasar data transformed from fluxes to unanchored luminosity distances via equation (7) along with the uncertainties obtained according to error propagation. These calibrated, unanchored quasar luminosity distances comprises the data set that we use to make inferences about cosmology in later sections.

On the other hand, in order to test the consistency between the calibrated quasar sample and the unanchored luminosity distance from SN Ia, we adopt the best-fitting values of the three quasar parameters to estimate the normalized residual of $\log(F_{\rm X})^{\rm SN}$ from equation (5) with respect to the measurement of $\log(F_{\rm X})$ following:

$$\Delta\log(F_{\rm X}) = \frac{\log(F_{\rm X})^{\rm SN} - \log(F_{\rm X})^{\rm QSO}}{\sqrt{\sigma^2_{\log(F_{\rm X})} + \gamma^2\sigma^2_{\log(F_{\rm UV})} + \delta^2}}. \tag{8}$$

The result for the residual is shown in Fig. 3. As can be seen from the right plot of Fig. 3, the distribution of the normalized residual is a Gaussian distribution, which indicates that $\log(\mathrm{F_X})$ data derived from the best-fitting values of the quasar parameters in our approach is consistent with $\log(\mathrm{F_X})$derived from supernovae data. Finding no evidence against the linear $\log(F_{\rm UV})$–$\log(F_{\rm X})$ relation the calibration method described above (based on Type Ia supernovae that we consider to be standardized candles) results in a well-behaved data set showing internal consistency (the residuals are Gaussian distributed). We then use this calibrated data set to reconstruct the expansion history.

4 ΛCDM INFERENCES

With the best-fitting quasar parameters, we have transformed the quasar fluxes into a set of unanchored luminosity distances, which we can now use to constrain the ΛCDM model (or any other cosmological model). In the flat-ΛCDM model, the unanchored luminosity distance can be written as,

$$D_{\rm L}H_0 = c(1+z)\int_0^z \frac{dz}{\sqrt{\Omega_{\rm m}(1+z)^3 + (1-\Omega_{\rm m})}}, \tag{9}$$

where $\Omega_{\rm m}$ is the current matter density. With this equation we can calculate $\log(D_{\rm L}H_0)^{\Lambda\rm CDM}$. The likelihood for the calibrated quasar distance data set $\left(\log(D_{\rm L}H_0)_i^{\rm QSO}\right)$ is then defined as

$$\ln\mathcal{L} = -\frac{1}{2}\sum_i\left[\frac{\left(\log(D_{\rm L}H_0(\Omega_m))_i^{\Lambda\rm CDM} - \log(D_{\rm L}H_0)_i^{\rm QSO}\right)^2}{\sigma^2_{\log(D_{\rm L}H_0);i}}\right]. \tag{10}$$

With this likelihood function we can then calculate the posterior for $\Omega_{\rm m}$ for both the entire calibrated quasar data set, and the subsample of quasars which consists of 2066 quasars with redshifts up to the largest redshift of SN Ia ($z = 2.3$). The constraints on $\Omega_{\rm m}$ are shown in Fig. 4. With the full quasar sample, we get $\Omega_m = 0.382^{+0.045}_{-0.042}$ and with the subsample we get $\Omega_m = 0.306^{+0.046}_{-0.042}$. The best-fitting result of $\Omega_{\rm m}$ from the subsample of quasars is highly consistent with the results from Risaliti & Lusso (2019) ($\Omega_{\rm m} = 0.31 \pm 0.05$). However, the fits on the matter density parameter from the full quasar sample show significant deviations from the value of $\Omega_{\rm m} = 0.3$. The fact that we could recover $\Omega = 0.306$ from the subsample of the calibrated quasar data set is relatively trivial, considering the fact that the quasars are calibrated with the Pantheon compilation which also infers $\Omega_{\rm m} \sim 0.3$ in the framework of flat-ΛCDM model. Hence, it makes no surprise that the calibrated quasar data set returns the same value when using only the quasars in the range of the Pantheon data set. What is more interesting is the quasars at higher redshift will shift

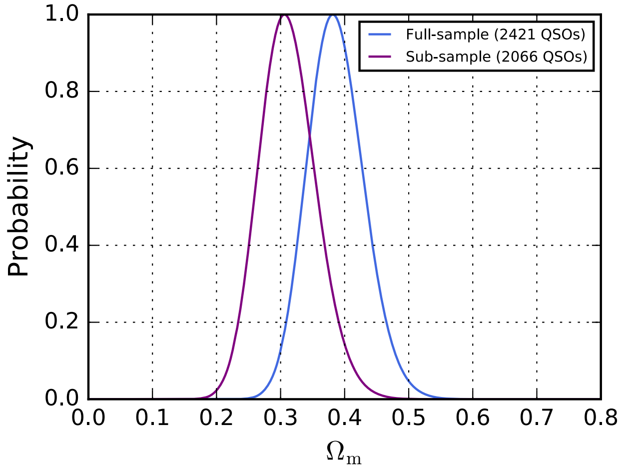

Figure 4. Constraints for a flat ΛCDM model from the calibrated quasar sample using both the full sample (blue) and the subsample (purple) of 2066 quasars with redshifts up to the maximum SN Ia redshift ($z \leq 2.26$).

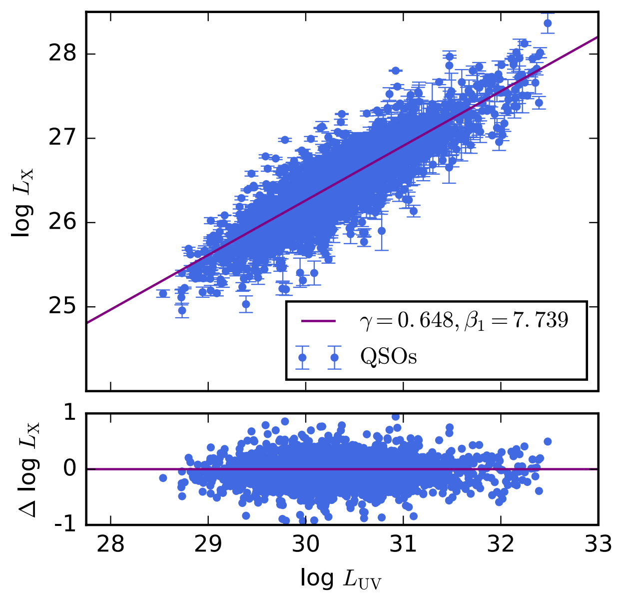

Figure 5. The linear relation between $\log(L_{\rm UV})$ and $\log(L_{\rm X})$ for the 2421 quasar sample we used. The purple solid line presents the best fit from our calibration results with slope $\gamma = 0.648$. The lower panel shows the residual, $\Delta\log(L_{\rm X})$ with respect to the best-fitting results.

the best-fitting $\Omega_{\rm m}$ to higher values, when the full quasar sample is taken into account.

Based on the best-fitting results from flat ΛCDM model, we can calculate the luminosity of the quasars from their flux measurements and the luminosity distances from the ΛCDM model with $\Omega_{\rm m}$ = 0.382, $\Omega_{\rm K}$ = 0 for the full sample of 2421 quasars. The results are shown in Fig. 5, and the purple solid line is calculated from the best-fitting quasar parameters from our calibration results. The lower panel shows the residuals $\Delta\log(L_{\rm X})$, with respect to the best-fitting quasar parameters. Fig. 5 demonstrate the linear relation between $\log(L_{\rm UV})$ and $\log(L_{\rm X})$ for quasars based on our calibration results and assumption of the standard ΛCDM model. While visually everything seems to be consistent with each other, more quantitative inspections are needed to check the consistency of the ΛCDM model and the data at the higher redshifts (redshifts beyond the range of the calibration).

5 GP RECONSTRUCTION AND CONSISTENCY TEST

In this section, we reconstruct the unanchored luminosity distances D_LH_0, the corresponding expansion history $h(z)$, and also the 'om diagnostic' $om(z) = \frac{h^2(z)-1}{(1+z)^3-1}$ (Sahni, Shafieloo & Starobinsky 2008) from the calibrated quasar sample with GP regression. We use the ΛCDM model that best fits the Pantheon data as a mean function in this GP analysis. These reconstruction results are shown in Fig. 6.

From these figures, we can see a noticeable evolution of these cosmological functions. By construction, the reconstruction matches the Pantheon expectation in the redshift regime with the highest density of SN Ia ($z \lesssim 1$). But beyond this redshift regime, the quasars prefer smaller distances than the ΛCDM fit to the Pantheon SN Ia would predict. As can be seen in the plot of the om diagnostic (Fig. 4), the reconstructed evolution of this probe is arising from the same features in the data that drive shift in the inferred matter density within ΛCDM. The evolution of the expansion history with redshift is more apparent in the GP reconstructions of Fig. 6 than in the ΛCDM inference of Fig. 4 basically because ΛCDM is relatively inflexible compared to GP regression. The kind of evolution in the expansion history needed to fit the full sample of the quasar data cannot be found in the ΛCDM model and shifting $\Omega_{\rm m}$ to higher values is merely a less bad fit to the data, rather than an objectively good fit. Rather, this sort of evolution would require an evolution in the dark energy. We seek to be agnostic about the preferred interpretation of these reconstructions, namely, whether this indicates a beyond-ΛCDM evolution of the expansion history, some evolution in the quasar luminosity calibration hyperparameters (β, γ) or a need for additional flexibility beyond the assumed linear relation between the log of the quasars' X-ray and UV luminosities. We leave this investigation for future work.

Rather than a visual inspection of the reconstructions, a more robust test to tell if any reconstructed, beyond-ΛCDM evolution is significant is to look at the posterior of the GP hyperparameters. The values of the hyperparameters play an important role in GP regression, so they are not fixed to a certain value during our GP regression. In fact, the posterior of the GP hyperparameters carries important information (Shafieloo et al. 2012; Shafieloo et al. 2013; Aghamousa et al. 2017; Keeley et al. 2020). If σ_f is consistent with zero it means that there is no significant evidence for deviations from the mean function. If ℓ is very small this may indicate that one is overfitting noise in the data, while if it is too large this mean that the data is uninformative about the expansion history. If the posterior for hyperparameters picks out a value for σ_f larger than 0, then the calibrated quasar sample contains information disfavouring the mean function. In Fig. 7, we show the posterior of GP hyperparameters with flat ΛCDM as mean function, the results show a $2-3\sigma$ deviation from 0, which indicates a preference for a beyond–ΛCDM evolution. The difference between this $2-3\sigma$ deviation from ΛCDM model based on Planck values ($\Omega_{\rm m} = 0.3$) and the 4σ deviation reported by Risaliti & Lusso (2019) from flat-ΛCDM family (different values of $\Omega_{\rm m}$) can be entirely attributed to the difference in methodology (Gaussian process regression versus parametric fitting). It is well-known that parametric fitting can have artificially tight constraints and can be biased towards particular forms (Maor, Brustein & Steinhardt 2001; Weller & Albrecht 2002; Huterer & Starkman 2003; Jönsson et al. 2004; Shafieloo et al. 2006; Shafieloo 2007). This is why we prefer GP or similar reliable model-independent methods.

In Khadka & Ratra (2021), the authors showed that QSOs at $z < 1.5-1.7$ are broadly consistent with ΛCDM model but deviations occurred above there and these high-redshift deviations cannot be

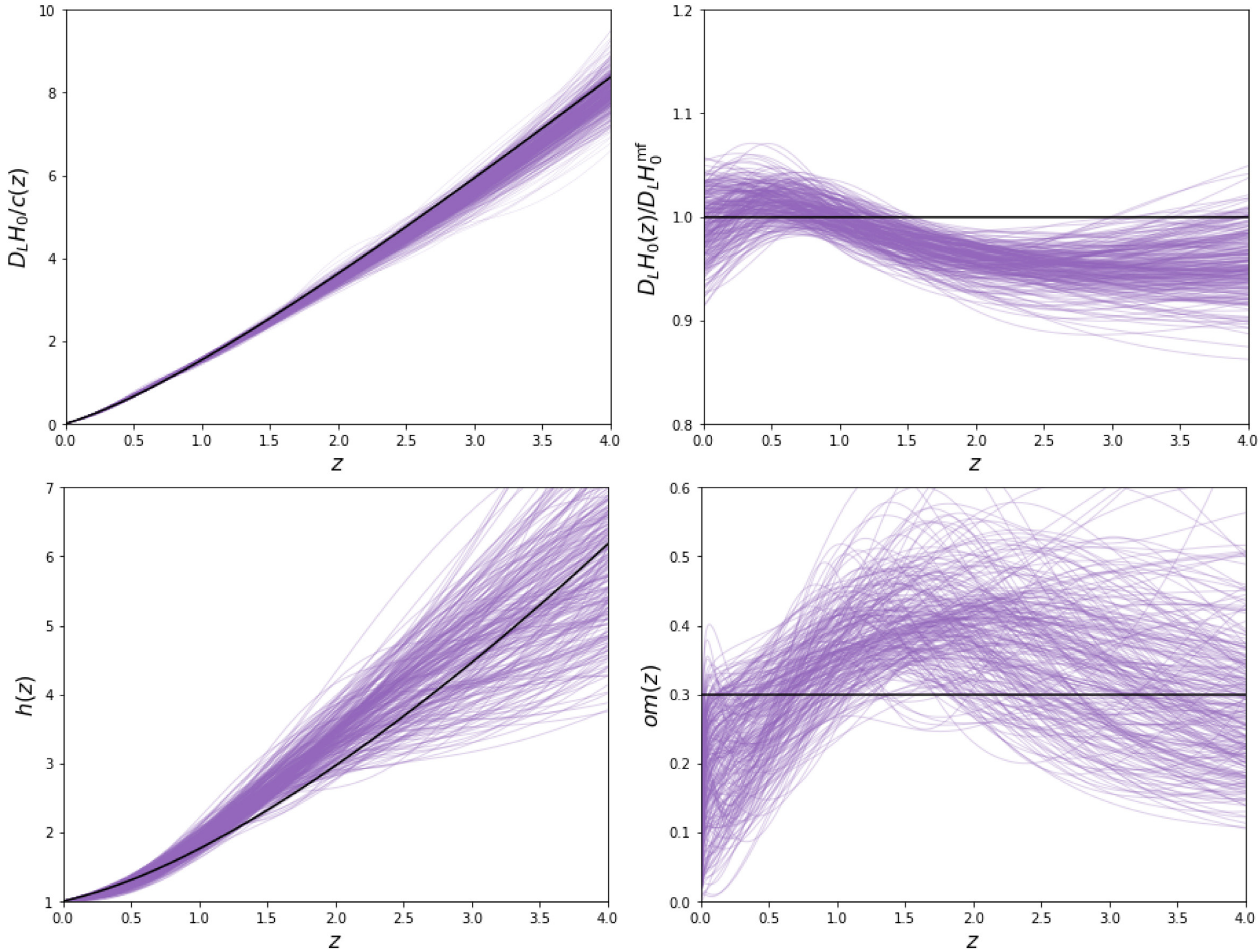

Figure 6. GP reconstructions with ΛCDM as the mean function. Each purple line shows a GP reconstruction with a χ^2 better than the best-fitting ΛCDM to the calibrated quasar data set. The black lines correspond to the mean function. The upper two panels show reconstructed $D_L H_0(z)$ functions and those same functions divided by the mean function (ΛCDM model that best fits the Pantheon SN Ia data). The bottom panels show $h(z)$ and om(z).

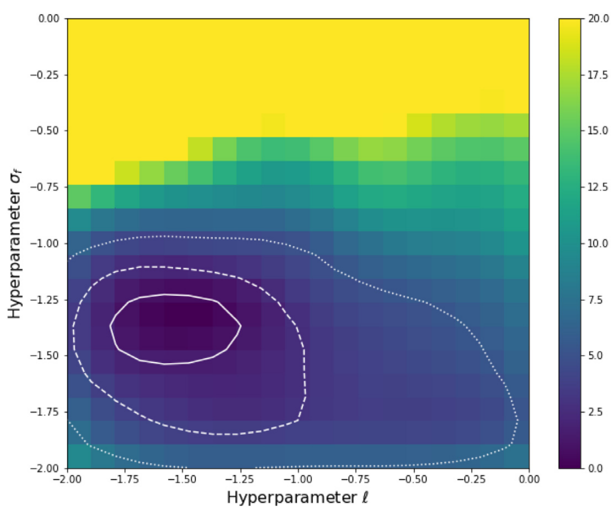

Figure 7. Posterior of the GP hyperparameters calibrated on QSO data using the SN Ia best-fitting ΛCDM model as a mean function. Colour scale corresponds to the $-\Delta\log$ Likelihood, while the white contours delimit the 68.3 per cent, 95.4 per cent, and 99.7 per cent confidence regions.

explained by any of their set of beyond-ΛCDM models. Based on this, they concluded that the QSO's UV–X-ray luminosity relation must evolve with redshift at higher redshift. We found similar results, except our model independent methods can construct examples of beyond-ΛCDM evolution that can explain the QSO data. Thus, we argue that there are a number of explanations for these high-redshift deviations in the QSO data set, either that it is new physics or an evolution in the calibration parametrization. All in all, our results show the same features in the QSO data as the work done by Khadka & Ratra (2021) but we have a broader interpretation of these features.

6 CONCLUSIONS

The quasar parameters γ, β, and δ are calibrated in a novel model-independent manner, where the degeneracy between these parameters and the expansion history of the Universe is broken by using the unanchored luminosity distances $D_L H_0$ reconstructed from the Pantheon SN Ia data with GP regression and the most recent quasar sample collected in Lusso et al. (2020). We confirm that quasars can be used as a cosmic probe based on the linear relation between log of the UV and X-ray luminosities assuming non-evolution with redshift for this relation. We also test the reliability of our calibration results by calculating the normalized residuals of $\log F_X$ with respect to SN Ia sample. The Gaussian distribution of the normalized residual shows the reliability of the calibration results.

Furthermore, we constrain the standard ΛCDM model with the calibrated quasar sample, which yields $\Omega_\mathrm{m} = 0.382^{+0.045}_{-0.042}$ for the full sample and $\Omega_\mathrm{m} = 0.306^{+0.046}_{-0.042}$ for the subsample. These constraints on Ω_m are consistent with previous results by Risaliti & Lusso (2015, 2019). For the subsamples, we get $\Omega_\mathrm{m} = 0.306^{+0.046}_{-0.042}$ which is in agreement with Risaliti & Lusso (2019) who find $\Omega_\mathrm{m} = 0.31 \pm 0.05$ when they analyse the $z < 1.4$ quasar data set. For the full sample, we also find deviations from ΛCDM, as does Risaliti & Lusso (2019), although with different significance due to the methodology. The expansion history can be reconstructed from the calibrated quasar sample with GP regression without any assumption about the true expansion history. The reconstructed expansion history seems evolving relative the SN Ia predictions, especially at high redshift. This appears to be the same evolution as seen in Risaliti & Lusso (2019) and Lusso et al. (2020), where they find the Hubble diagram of quasars is well fit by the flat ΛCDM model at redshifts $z < 1.4$ but notice deviations occur above there. Our model-independent (non-parametric) method that finds similar results shows additionally that this deviation is not merely a feature of the choice of parametrization but a real feature of the data set.

Finally, this 2–3σ preference for a beyond-ΛCDM evolution is also seen in the posterior probability distribution of the GP hyperparameters where the preference for $\sigma_f > 0$ indicates that the data holds more information than can be modelled by the input mean function (where we assumed the best-fitting ΛCDM model as the mean function). Whether this information is truly indicative of beyond-ΛCDM physics or a systematic effect is uncertain, and we seek to answer this question in future works. In fact some evolution in the quasar luminosity calibration hyperparameters (β, γ) or a need for additional flexibility beyond the assumed linear relation between the log of the quasars' X-ray and UV luminosities can be also considered as alternative reasons for the observed evolution.

Summarizing, using quasars as standardizable candles can fill the redshift gap between farthest observed SN Ia and CMB measurements substantially and improve the constraints on cosmological models at $z > 2$. Future surveys including *Euclid*, LSST, and other possible surveys will certainly provide more quasar samples. With these samples, it will be possible to have a much more precise constraint on cosmological models.

ACKNOWLEDGEMENTS

XL was supported by National Natural Science Foundation of China under grant nos 12003006, 11947091; Hebei NSF under grant no. A2020205002, and the fund of Hebei Normal University under grants no. L2020B02. AS would like to acknowledge the support of the Korea Institute for Advanced Study (KIAS) grant funded by the Korea government. SC and Z-HZ were supported by National Key R&D Program of China No. 2017YFA0402600; the National Natural Science Foundation of China under grant nos 12021003, 11690023, 11633001, 11920101003, and 11373014; Beijing Talents Fund of Organization Department of Beijing Municipal Committee of the CPC; the Strategic Priority Research Program of the Chinese Academy of Sciences, grant no. XDB23000000; and the Interdiscipline Research Funds of Beijing Normal University. MB was supported by the Key Foreign Expert Program for the Central Universities No. X2018002. This work benefits from the high performance computing clusters at College of Physics, Hebei Normal University.

DATA AVAILABILITY

The data underlying this article will be shared on reasonable request to the corresponding author.

REFERENCES

Aghamousa A., Hamann J., Shafieloo A., 2017, J. Cosmol. Astropart. Phys., 2017, 031
Aghanim N. et al., 2020, A&A, 641, A6
Avni Y., Tananbaum H., 1986, ApJ, 305, 83
Cao S., Zheng X., Biesiada M., Qi J., Chen Y., Zhu Z.-H., 2017a, A&A, 606, A15
Cao S., Biesiada M., Jackson J., Zheng X., Zhao Y., Zhu Z.-H., 2017b, J. Cosmol. Astropart. Phys., 2017, 012
Cao S., Biesiada M., Qi J., Pan Y., Zheng X., Xu T., Ji X., Zhu Z.-H., 2018, Eur. Phys. J. C, 78, 749
Evans I. N. et al., 2010, ApJS, 189, 37
Foreman-Mackey D., Hogg D. W., Lang D., Goodman J., 2013, Publ. Astron. Soc. Pac., 125, 306
Geng S., Cao S., Liu T., Biesiada M., Qi J., Liu Y., Zhu Z.-H., 2020, ApJ, 905, 54
Holsclaw T., Alam U., Sanso B., Lee H., Heitmann K., Habib S., Higdon D., 2010a, Phys. Rev. D, 82, 103502
Holsclaw T., Alam U., Sanso B., Lee H., Heitmann K., Habib S., Higdon D., 2010b, Phys. Rev. Lett., 105, 241302
Holsclaw T., Alam U., Sansó B., Lee H., Heitmann K., Habib S., Higdon D., 2011, Phys. Rev. D, 84, 083501
Huterer D., Starkman G., 2003, Phys. Rev. Lett., 90, 031301
Jönsson J., Goobar A., Amanullah R., Bergström L., 2004, J. Cosmol. Astropart. Phys., 2004, 007
Joudaki S., Kaplinghat M., Keeley R., Kirkby D., 2018, Phys. Rev. D, 97, 123501
Keeley R. E., Joudaki S., Kaplinghat M., Kirkby D., 2019, J. Cosmol. Astropart. Phys., 2019, 035
Keeley R. E., Shafieloo A., L'Huillier B., Linder E. V., 2020, MNRAS, 491, 3983
Keeley R. E., Shafieloo A., Zhao G.-B., Vazquez J. A., Koo H., 2021, AJ, 161, 151
Kelly B. C., 2007, AJ, 665, 1489
Khadka N., Ratra B., 2020a, MNRAS, 492, 4456
Khadka N., Ratra B., 2020b, MNRAS, 497, 263
Khadka N., Ratra B., 2021, MNRAS, 502, 6140
Li X., Cao S., Zheng X., Qi J., Biesiada M., Zhu Z.-H., 2017, Eur. Phys. J. C, 77, 677
Liao K., Shafieloo A., Keeley R. E., Linder E. V., 2019, ApJ, 886, L23
Liao K., Shafieloo A., Keeley R. E., Linder E. V., 2020, ApJ, 895, L29
Liu T., Cao S., Zhang J., Biesiada M., Liu Y., Lian Y., 2020a, MNRAS, 496, 708
Liu T., Cao S., Biesiada M., Liu Y., Geng S., Lian Y., 2020b, ApJ, 899, 71
Liu Y., Cao S., Liu T., Li X., Geng S., Lian Y., Guo W., 2020c, ApJ, 901, 129
Lusso E., Risaliti G.,Nardini E., et al., 2020, A&A, 642, A150
Lusso E., 2020, Front. Astron. Space Sci., 7, 8
Lusso E., Risaliti G., 2016, ApJ, 819, 154
Lusso E., Risaliti G., 2017, A&A, 602, A79
Lusso E., Piedipalumbo E., Risaliti G., Paolillo M., Bisogni S., Nardini E., Amati L., 2019, A&A, 628, L4
Maor I., Brustein R., Steinhardt P. J., 2001, Phys. Rev. Lett., 86, 6
Menzel M.-L. et al., 2016, MNRAS, 457, 110
Mingo B. et al., 2016, MNRAS, 462, 2631
Mortlock D. J. et al., 2011, Nature, 474, 616
Nardini E., et al., 2019, A&A, 632, A109
Pâris I. et al., 2017, A&A, 597, A79
Qi J.-Z., Cao S., Zhang S., Biesiada M., Wu Y., Zhu Z.-H., 2019, MNRAS, 483, 1104
Qi J.-Z., Zhao J.-W., Cao S., Biesiada M., Liu Y., 2021, MNRAS, 503, 2179
Rasmussen C. E., Williams C. K. I., 2006, The MIT Press, Cambridge, Massachusetts London, England

Risaliti G., Lusso E., 2015, ApJ, 815, 33
Risaliti G., Lusso E., 2017, Astron. Nachr., 338, 329
Risaliti G., Lusso E., 2019, Nature Astron., 3, 272
Sahni V., Shafieloo A., Starobinsky A. A., 2008, Phys. Rev. D, 78, 103502
Salvestrini F., Risaliti G., Bisogni S., Lusso E., Vignali C., 2019, A&A, 631, A120
Scolnic D. M. et al., 2018, ApJ, 859, 101
Shafieloo A., 2007, MNRAS, 380, 1573
Shafieloo A., Alam U., Sahni V., Starobinsky A. A., 2006, MNRAS, 366, 1081
Shafieloo A., Kim A. G., Linder E. V., 2012, Phys. Rev. D, 85, 123530
Shafieloo A., Kim A. G., Linder E. V., 2013, Phys. Rev. D, 87, 023520
Webb N. A. et al., 2020, A&A, 641, A136
Weller J., Albrecht A., 2002, Phys. Rev. D, 65, 103512
Zheng X., Cao S., Biesiada M., Li X., Liu T., Liu Y., 2021, Sci. China Phys. Mech. Astron., 64, 259511

This paper has been typeset from a TEX/LATEX file prepared by the author.